Progress in Additive Manufacturing (2020) 5:3–9
https://doi.org/10.1007/s40964-020-00117-7

FULL RESEARCH ARTICLE

Laser powder bed fusion of Nd–Fe–B permanent magnets

Florian Bittner[1] · Juliane Thielsch[1] · Welf-Guntram Drossel[1,2]

Received: 13 January 2020 / Accepted: 7 February 2020 / Published online: 20 February 2020

Abstract
In this work, we use laser powder bed fusion (LPBF) to produce Nd–Fe–B magnets. A suitable process window is developed, which allows to fabricate isotropic samples with outstanding magnetic performance. The sample quality is mainly defined by the energy input during LPBF and sintering or delamination occurs, if the process parameter are improperly adjusted. Magnetic and structural properties become better as energy input increases, until the material-specific limit for processability has been reached. Magnets with coercivity of 886 kA/m ($\mu_0 H_c = 1.1$ T) and maximum energy product of 63 kJ/m^3 can be produced from Nd-lean commercial powder without any post treatment. Thereby, our samples represent the new benchmark for permanent magnets produced by additive manufacturing. On the example of coercivity, the impact of laser power, scan velocity and hatch spacing is discussed. It is shown that coercivity can be sufficiently well described by a simple phenomenological model.

Keywords Laser powder bed fusion (LPBF) · Nd–Fe–B · Permanent magnets · Functional materials · Magnetic materials · Coercivity

1 Introduction

Laser powder bed fusion (LPBF) for generation of metal parts is becoming an established processing technique for individualized products and small series displaying structural complexity and short time-to-market. However, it is at the moment limited to a few structural metals like steels, aluminum and titanium alloys [1]. For metallic functional materials, only shape memory alloys based on NiTi and NiTiHf received considerable scientific interest so far [2, 3]. The current development state of additive manufacturing of magnetic materials is actually limited to some proof of principle studies.

Permanent magnets are used in electrical engines to provide a magnetic flux without the application of an electric current. Furthermore, permanent magnets require sufficient resistance against demagnetization in a reversed magnetic field. The basic properties of permanent magnets are remanent polarization J_r, which corresponds to the magnetic field created by the magnet, and coercivity H_c, which denotes the magnetic field that is needed to demagnetize a magnet. Remanence and coercivity are both determine the maximum energy product $(BH)_{max}$, which acts as figure of merit for permanent magnets. Thereby, if coercivity of a magnet is sufficiently large ($H_c > {}^1/_2 J_r$), $(BH)_{max}$ is in the first approximation determined by remanence ($(BH)_{max} \sim J_r^2$).

Since the development of Nd–Fe–B in 1984 [4, 5] it became the most advanced permanent magnet material and is nowadays used for recording devices, holdings, electrical motors or wind turbines [6]. Nd–Fe–B permanent magnets receive their superior magnetic performance from the hard magnetic $Nd_2Fe_{14}B_1$ intermetallic phase as well as careful chemical and microstructural design. Conventionally, magnet production is realized by powder metallurgical route consisting of powder fabrication, pressing and magnetic field alignment, sintering and post sintering heat treatment. With this technique, design freedom is limited to cylinders, cubes or cuboids, rings and ring segments and $(BH)_{max}$ can reach up to 474 kJ/m^3 [7]. If a higher degree of geometrical flexibility is necessary, bonded magnets can be used. Hereby, Nd–Fe–B powders are mixed with polymer, typically Polyamid 11 or 12, and shaped by compression molding or injection molding [8]. In case of polymer bonded magnets, the volume of magnetic active material is

✉ Florian Bittner
florian.bittner@iwu.fraunhofer.de

[1] Fraunhofer Institute for Machine Tooling and Forming Technologies IWU, Dresden, Germany

[2] Chemnitz Technical University, Chemnitz, Germany

reduced to 50–85%, which results in a remarkable reduction of $(BH)_{max}$ to 30–85 kJ/m^3 [8]. Furthermore, fabrication of bonded magnets underlie the typical geometric restrictions of polymer shaping methods and following processing and application is limited to the thermal stability of Polyamid.

Additive manufacturing of polymer bonded permanent magnets was used to overcome that geometrical restrictions and several AM techniques have been used so far: Fused Filament Fabrication [9], Binder Jetting [10], Selective Laser Sintering [11] and Melt Extrusion [12]. Alternatively, LPBF can be used to produce bulk magnets [13–17]. LPBF of Nd–Fe–B has the potential to combine geometrical freedom with improved magnetic performance by increasing the volume content of magnetic material since a polymer binder is not necessary.

The aim of this paper is to demonstrate the processability of commercial Nd–Fe–B powder at a LPBF machine, which represents the industrial standard. The complex interplay between LPBF process parameter and resulting magnetic properties is analyzed and a first phenomenological model is developed to show the influence of LPBF on coercivity of Nd–Fe–B magnets.

2 Experimental

Nd–Fe–B powder (MQP-S, Magnequench [18]), which is the only commercially available Nd–Fe–B powder with spherical morphology, was used in this work. The powder has Nd-lean composition and was initially optimized for fabrication of isotropic polymer bonded magnets by injection molding. As LPBF requires a powder particle size below 40 µm, the original powder was sieved and only the fraction < 40 µm was used for further experiments. The particle size distribution of the original and sieved powder was determined by dynamic image analysis using a Camsizer X2 (Retsch GmbH). For sample preparation, a commercial M2 LPBF machine from ConceptLaser was used, which is equipped with a 400 W diode pumped fiber laser (wavelength 1070 nm) with a spot size of 110 µm. LPBF was performed under Ar atmosphere with O_2 content below 0.5% to prevent oxidation with a layer thickness of 30 µm on a steel substrate. It was not possible to melt single tracks with a height of several layers due to crack formation caused by the brittle behavior of the intermetallic magnetic material. To find a suitable process window for bulk specimen cylindrical samples (diameter 5 mm, height 5 mm) were produced, whereby laser power, scan velocity and hatch spacing were altered between 50 and 150 W, 1000 and 2500 mm/s and 35 and 75 µm, respectively.

After optical inspection the specimen were removed from the substrate and their magnetic properties were measured using a Permeagraph (Magnetphysik GmbH) with maximum applied field of 2.3 T at room temperature. Morphology and composition of the Nd–Fe–B powder was analyzed using a scanning electron microscope (SEM) Zeiss Supra 25, which is equipped with an energy dispersive X-ray spectrometer (EDX).

3 Results and discussion

3.1 Characteristics of the initial powder

To the best of our knowledge, the only commercial available Nd–Fe–B powder with spherical morphology is MQP-S from Magnequench. Independently from the existing data sheet [18] the powder was analyzed in terms of particle size, composition and magnetic performance.

The particle size distribution of the original powder and subsequently sieved to < 40 µm is shown in Fig. 1a. The original powder has a d_{50} and d_{90} value of 39 and 59 µm, respectively. Since the powder was originally not designed for LPBF the particle size distribution is not ideal. After sieving the initial powder the particle size distribution is shifted towards smaller values and d_{50} and d_{90} values are reduced to of 32 and 46 µm, respectively. Even the selectivity seems not optimal, e.g. more than 10% of the powder is still larger than 40 µm, the powder fulfills now the requirements of the LPBF process.

The shape of the Nd–Fe–B powder is almost ideal spherical (Fig. 1b) and no satellites can be found. The composition was determined by EDX to be Fe70.8–Nd18.2–Zr4.3–Co2.4–Ti2.2–Pr2.1 (composition in wt%), which corresponds to a Nd-lean composition as Nd–Fe–B sintered magnets typically have (Nd + Pr) contents of more than 30 wt%.

3.2 Process window for successful fabrication of Nd–Fe–B magnets by LPBF

The hard magnetic main phase of Nd–Fe–B magnets, $Nd_2Fe_{14}B_1$, has a complex tetragonal crystallographic unit cell containing 68 atoms. Related to the crystallographic complexity, Nd–Fe–B shows different mechanical and thermo-physical properties compared to structural LPBF materials such as steels, Al- and Ni-based alloys. The differences are, for example, visible in lower thermal conductivity and lower and anisotropic thermal expansion [19]. Furthermore, Nd–Fe–B behaves mechanically brittle, which is visible in fracture toughness of approximately 3.8 MPa/$\sqrt{m}$ [20] and impact toughness of 2.7–5 × 10^{-3} J/cm^2 [21], while for steels 50 MPa/$\sqrt{m}$ [22] and 60–350 J/cm^2 [23] are common. From these metallurgical features, it is assumed, that Nd–Fe–B will behave different during LPBF compared to established LPBF materials.

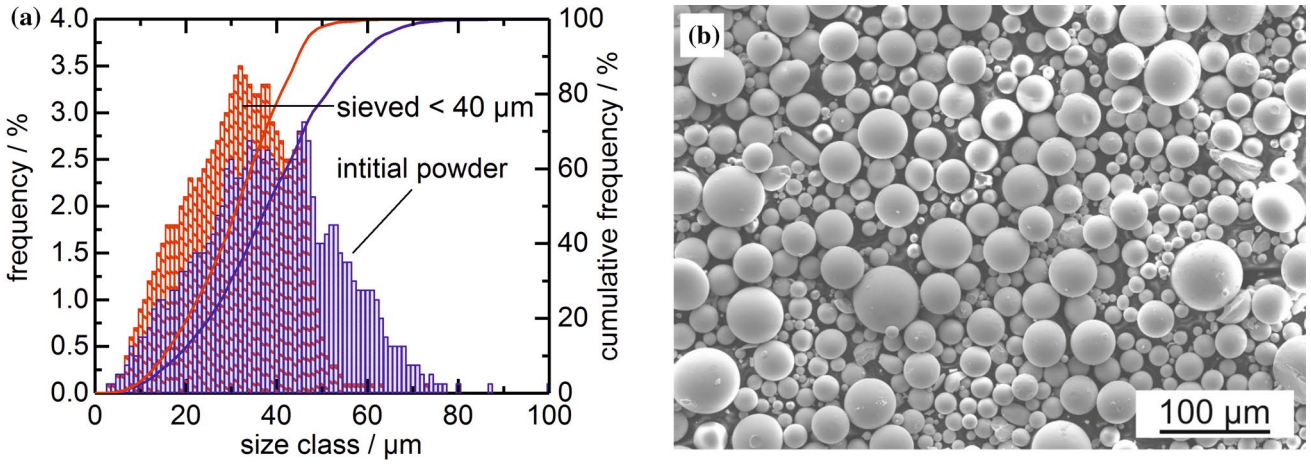

Fig. 1 **a** Particle size distribution (minimum particle width) of as received and after sieving to < 40 µm and **b** SEM image of sieved Nd–Fe–B powder

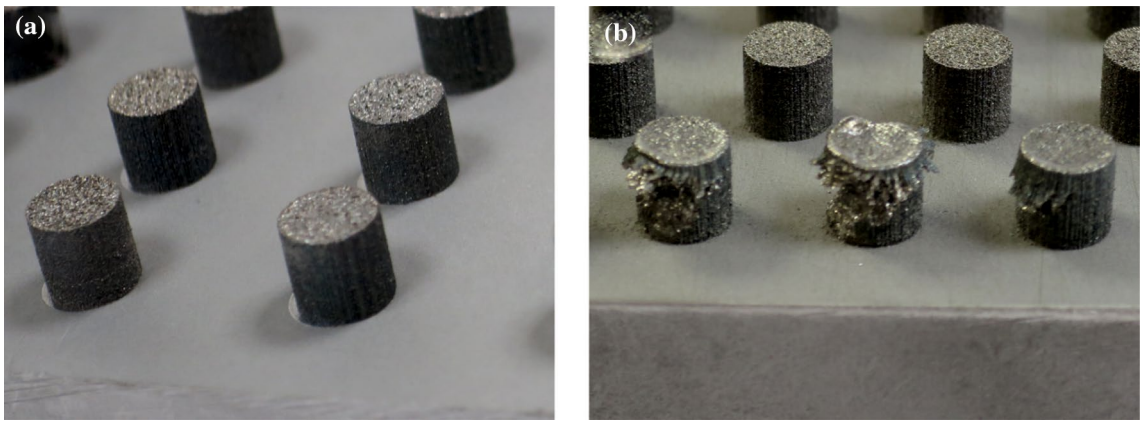

Fig. 2 Examples of LPBF fabricated Nd–Fe–B samples: **a** cylindrical sample with suitable parameters, **b** delamination caused by too high energy input

To determine a suitable process window for successful generation of bulk Nd–Fe–B magnets by LPBF the influence of process parameter laser power P, scan velocity v_{scan} and hatch spacing h_y was studied. The cooperative influence of these parameters is captured by line energy E_L and area energy E_A, whereby both are defined as follows:

$$E_L = \frac{P}{v_{scan}} \tag{1a}$$

$$E_A = \frac{E_L}{h_y} = \frac{P}{v_{scan} \cdot h_y} \tag{1b}$$

For area energies below 0.6–0.8 J/mm^2 only sintering of powder particles is observed, which results in slightly consolidated highly porous samples. An increased area energy between 0.8 and 2.3 J/mm^2 results in a stable LPBF process, which generates outward intact bulk samples (Fig. 2a).

Thereby, the choice of laser power, scan velocity and hatch spacing is of minor importance, as long as the area energy lies within the process window. If the energy input is further raised, delamination is increasingly observed, which can be seen in Fig. 2b. Thereby, delamination occurs not between sample and substrate, but within the sample. Furthermore, it was found that laser power of 200 W or more is in general unsuitable for LPBF of Nd–Fe–B.

3.3 Magnetic properties of LPBF-generated Nd–Fe–B permanent magnets

From all tested scan parameter these were selected, which lie within the suitable process window, e.g. lead to intact samples. For each parameter set, several cylindrical samples were generated by LPBF and their magnetic properties were measured by a Permeagraph. Two examples for different magnetic performances are shown in Fig. 3 and compared

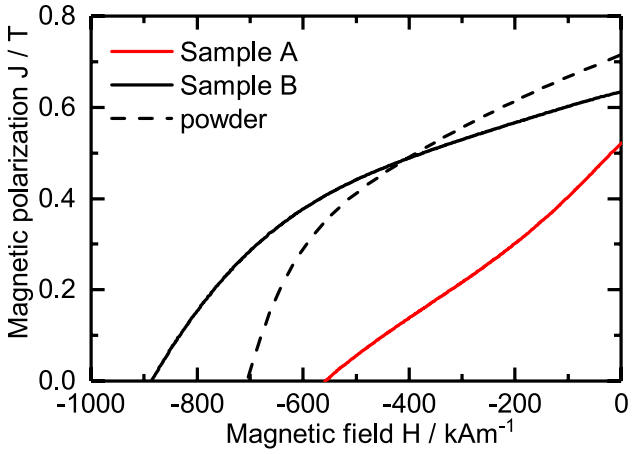

Fig. 3 Impact of process parameter on demagnetization curves of LPBF-fabricated Nd–Fe–B magnets in comparison to the initial powder. (Sample A and Sample B were generated with the same line energy but different hatch spacing)

to the demagnetization curve of the initially sieved powder. The powder with a particle size < 40 µm shows a remanence, J_r, of 0.71 T and coercivity, H_c, of 705 kA/m. By neglecting the non-consolidated nature of the powder, a maximum energy product, $(BH)_{max}$ of 72.6 kJ/m^3 is determined. The values of J_r and $(BH)_{max}$ for the sieved powder are slightly below the specified characteristics given by the data sheet [18] with 0.73–0.76 T and 80–92 kJ/m^3 for J_r and $(BH)_{max}$, respectively. A possible reason might be the removal of the coarse particle fraction by sieving.

LPBF affects the magnetic characteristics of the fabricated magnet drastically, which can be seen by the demagnetization curves "Sample A" and "Sample B" in Fig. 3. In both cases, line energy E_L was 0.067 J/mm^2, but hatch spacing was decreased from Sample A to Sample B from 75 to 35 µm. Sample A shows a moderate remanence and low coercivity of 0.52 T and 558 kA/m, respectively and a maximum energy product of only 28 kJ/m^3. The values are significantly below the characteristics of the initial powder. Reduced hatch spacing leads to enhancement of remanence and coercivity to 0.63 T and 886 kA/m^3, respectively, giving a maximum energy density of 63 kJ/m^3. It is worth noting, that magnetic performance resulting by this parameter set exceeds the properties, which are obtained from LPBF-generated Nd–Fe–B permanent magnets so far. A comparison of our results with literature data is given in Table 1. It is remarkable, that coercivity of the Nd-lean MQP-S powder can be increased up to almost 900 kA/m (more than 1.1 T)[1]

[1] Sometimes the magnetic field value coercivity is given in units of magntic flux density B or magnetic polarization J which is [T] (Tesla) and the conversion is $\mu_0 H_C$ ($\mu_0 = 4\pi * 10^{-7}$ N/A^2).

Table 1 Comparison of optimal magnetic properties achieved by LPBF of Nd–Fe–B in this work and literature values

	H_{ci} (kA/m)	B_r (T)
Nd–Fe–B powder	706	0.71
This study	886	0.63
Jacimovic et al. [14]	695	0.59
Huber et al. [15]	519	0.44
Urban et al. [17]	825	0.55

by LPBF. Recently, Huber et al. [15] used several rare earth-transion metal eutectics to enhance coercivity of LPBF processed samples by a subsequent grain boundary diffusion treatment. Thereby, they were able to raise coercivity from 517 to 857 kA/m by the addition of $Nd_{80}Cu_{20}$ to the as built sample. In our case, we found an even higher coercivity by a proper optimization of the LPBF process without a further post treatment.

Furthermore, the shape of the demagnetization curve is affected. Initial powder and Sample B show a typical curve of isotropic permanent magnets, which is characterized by a continuous and increasingly reduction of polarization with increasing negative magnetic field. However, Sample A shows a rapid decrease of polarization at low negative fields, which is typically caused by soft magnetic inclusions in the permanent magnetic microstructure with a size exceeding the coupling length for exchange spring magnets [24].

The influence of laser power and scan velocity for a fixed hatch spacing of 75 µm is shown in Fig. 4 for several properties. The aim for best magnetic performance is to maximize remanence and coercivity, which will also give an optimal maximum energy product. As can be seen from Fig. 4a–c, a general trend exists, that for enhanced energy input, either by reduced scan velocity or enhanced laser power, magnetic properties become considerably better. However, this trend is limited by the maximum energy input for LPBF-processing of Nd–Fe–B, as it was discussed earlier. For density (Fig. 4d) the mass of the samples was measured by a balance and divided by the volume. This gives only a rough estimation of density, but it shows the same trend as visible for magnetic properties.

Remanence of a permanent magnet is mainly determined by the volume content of permanent magnetic material and its crystallographic texture. For isotropic magnets fabricated from MQP-S powder, a remanence of 0.71 is expected, which is the value of the initial powder. For all studied combinations of laser power and scan velocity remanence is always below the value of the powder. However, the reduction can be explained by density, which has obviously not reached 100% for all samples. This assumption is supported by the comparable dependence of remanence and density from the scan parameter (Fig. 4a, d).

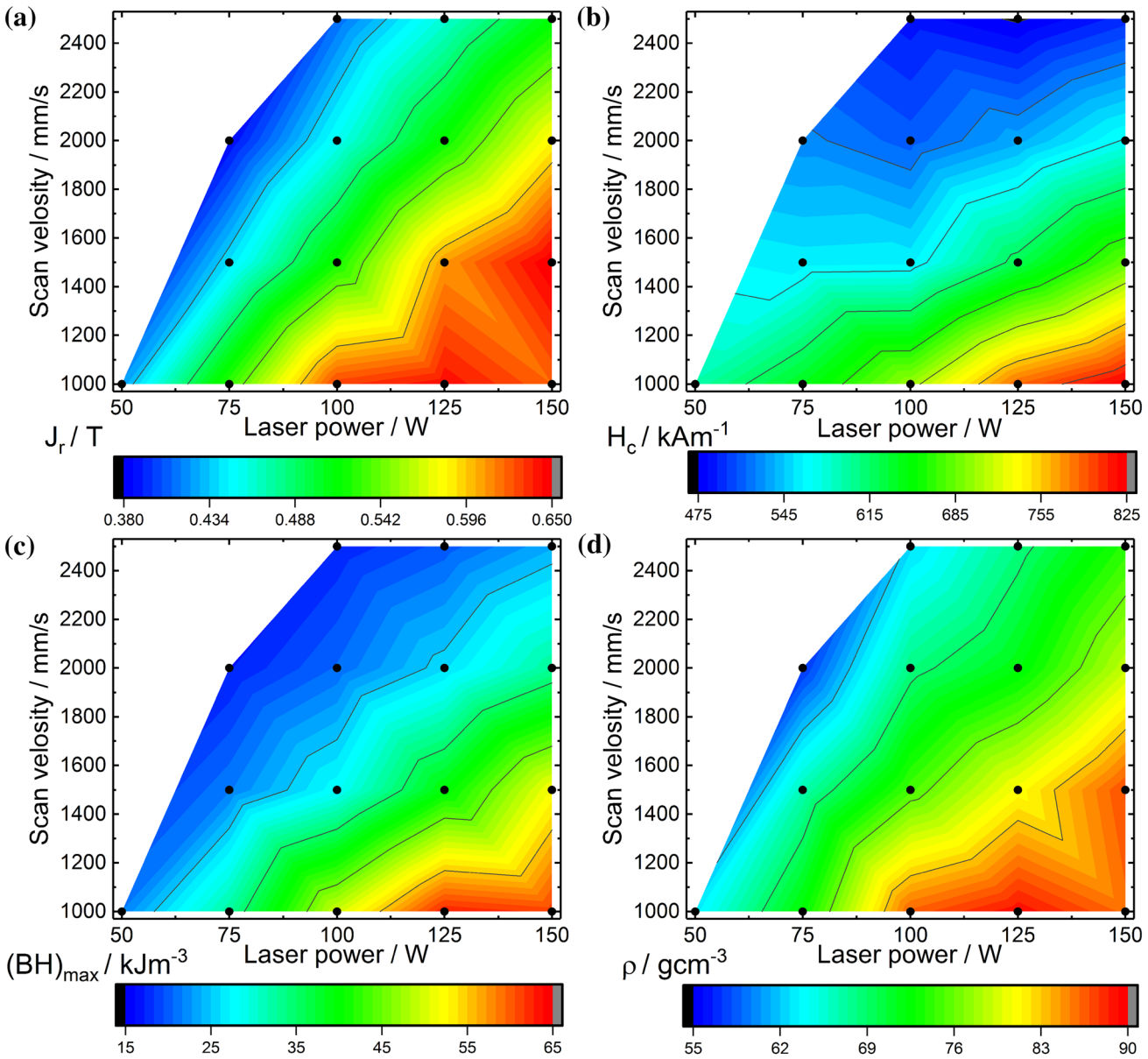

Fig. 4 Impact of laser power and scan velocity on magnetic properties **a** remanence J_r, **b** coercivity H_c, **c** maximum energy product $(BH)_{max}$ and **d** density of LPBF fabricated Nd–Fe–B magnets for a hatch spacing of 75 µm. The black circles represent tested parameter combinations

Thereby, it is concluded, that no strong crystallographic texture exists in our samples after LPBF and the samples behave magnetically isotropic.

The effect of laser power and scan velocity can be merged into line energy E_L, which is defined by Eq. (1a). The influence of line energy on coercivity for hatch spacings of 35 µm and 75 µm is shown in Fig. 5a. Coercivity shows a linear dependency from line energy, whereby the slope depends on the hatch spacing. The influence of laser power, scan velocity and hatch spacing on coercivity can be considered by the following formula:

$$\frac{H_c}{\mathrm{kA/m}} = H_c^0 - 3{,}83\frac{h_y}{\mu\mathrm{m}} + \frac{E_L}{\mathrm{J/mm}} \cdot \left(7740 - 59{,}18\frac{h_y}{\mu\mathrm{m}}\right) \tag{2}$$

H_c^0 represents a reference value of 626 kA/m. Please note, that the model is only of phenomenological nature and captures the influence of several LPBF parameter on coercivity. For this reason, the underlying physical mechanisms are not taken into account.

By application of Eq. (2) to the LPBF parameter displayed in Fig. 5a the model can be tested and a comparison of

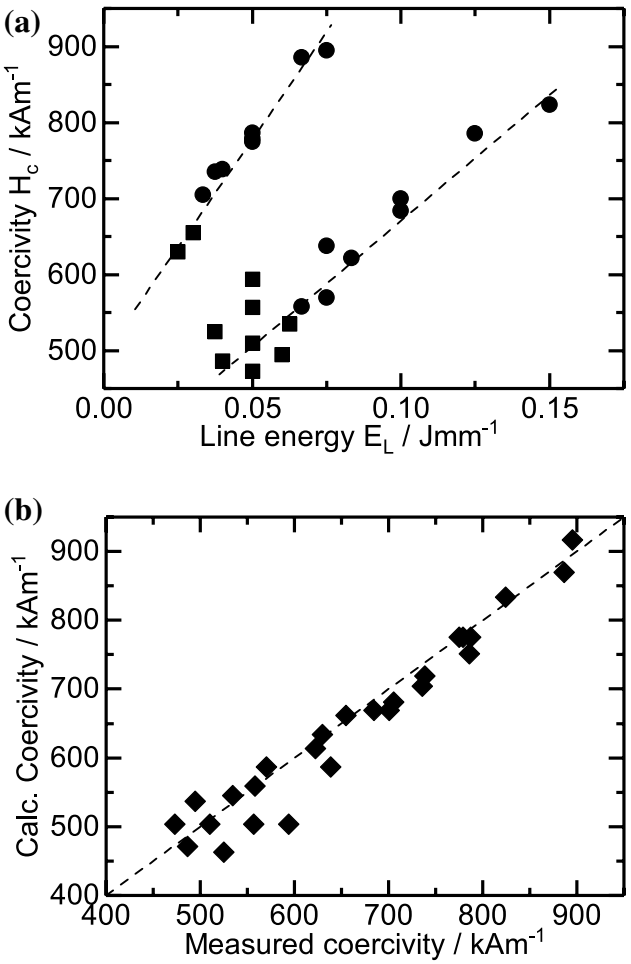

Fig. 5 **a** impact of line energy on coercivity for hatch spacing of 75 µm (circles) and 35 µm (squares) and **b** comparison of measured and calculated coercivity of LPBF fabricated Nd–Fe–B permanent magnets (dashed line is guide to the eye)

measured and calculated coercivity is shown in Fig. 5b. For coercivity of more than 600 kA/m the accordance between experimental and calculated values is noticeable fine. For lower coercivities some deviations are visible, which may be attributed to incomplete melting caused by low energy input. Especially for hatch spacing of 75 µm line energy of 0.05 J/mm represents the bottom limit of the previously defined process window. Furthermore, an enhancement of coercivity above 900 kA/m for the Nd-lean MQP-S powder is questionable, since the maximum energy input for LPBF is limited. If line energy E_L is increased further, delamination of the samples occurs.

4 Conclusion

In this work, we used laser powder bed fusion (LPBF) to produce Nd–Fe–B permanent magnets from commercial available Nd-lean powder with spherical morphology (MQP-S from Magnetquench). A suitable process window was identified by careful optimization of LPBF parameter. The resulted magnetic properties, remanence J_r of 0.63 T, coercivity H_c of 885 kA/m and maximum energy product $(BH)_{max}$ of 63 kJ/m^3, overcome published reference values significantly and represent the actual benchmark for additive manufacturing of permanent magnets. Furthermore, the magnetic performance of LPBF-fabricated samples is comparable or exceeds conventional polymer bonded permanent magnets. It was found, that the general processability is mainly determined by the area energy input during LPBF and a stable process is possible for an area energy between 0.6 and 2.3 J/mm^2. For lower values, low consolidation through sintering is observed, while higher energy leads to delamination. Magnetic properties and density shows a similar behavior of enhancement as laser power is increased or scan velocity or hatch spacing is decreased. However, the trend is limited by the maximum allowed energy input for LPBF for this material. A first phenomenological model considers the impact of LPBF parameter on coercivity. Since an unexpected high coercivity for Nd-lean precursor can be obtained by LPBF, this technology offers new opportunities for resource-efficient production of permanent magnets. Furthermore, LPBF seems to be able to create different magnetic properties in one sample directly during magnet shaping by a proper choice of process parameters, without further post treatment. This is not possible with any other available processing technology for permanent magnets. Investigations to clarify the interplay between processing, microstructure and resulting magnetic properties are in progress.

Acknowledgements Open Access funding provided by Projekt DEAL. Dr. Tobias Gustmann and Alexander Kahnt are kindly acknowledged for experimental assistance.

Funding The funding was provided by Fraunhofer-Gesellschaft within the internal Attract project "InMagMat".

Compliance with ethical standards

Conflict of interest The authors declare no conflict of interest.

References

1. Yap CY, Chua CK, Dong ZL et al (2015) Review of selective laser melting: materials and applications. Appl Phys Rev 2:41101. https://doi.org/10.1063/1.4935926
2. Elahinia M, Shayesteh Moghaddam N, Taheri Andani M et al (2016) Fabrication of NiTi through additive manufacturing: a review. Prog Mater Sci 83:630–663. https://doi.org/10.1016/j.pmatsci.2016.08.001
3. Elahinia M, Shayesteh Moghaddam N, Amerinatanzi A et al (2018) Additive manufacturing of NiTiHf high temperature shape memory alloy. Scr Mater 145:90–94. https://doi.org/10.1016/j.scriptamat.2017.10.016
4. Croat JJ, Herbst JF, Lee RW et al (1984) Pr-Fe and Nd-Fe-based materials: a new class of high-performance permanent magnets (invited). J Appl Phys 55:2078–2082. https://doi.org/10.1063/1.333571
5. Sagawa M, Fujimura S, Togawa N et al (1984) New material for permanent magnets on a base of Nd and Fe (invited). J Appl Phys 55:2083–2087. https://doi.org/10.1063/1.333572
6. McCallum RW, Lewis L, Skomski R et al (2014) Practical aspects of modern and future permanent magnets. Annu Rev Mater Res 44:451–477. https://doi.org/10.1146/annurev-matsci-070813-113457
7. Matsuura Y (2006) Recent development of Nd–Fe–B sintered magnets and their applications. J Magn Magn Mater 303:344–347. https://doi.org/10.1016/j.jmmm.2006.01.171
8. Ma BM, Herchenroeder JW, Smith B et al (2002) Recent development in bonded NdFeB magnets. J Magn Magn Mater 239:418–423
9. Huber C, Abert C, Bruckner F et al (2016) 3D print of polymer bonded rare-earth magnets, and 3D magnetic field scanning with an end-user 3D printer. Appl Phys Lett 109:162401. https://doi.org/10.1063/1.4964856
10. Paranthaman MP, Shafer CS, Elliott AM et al (2016) Binder jetting: a novel NdFeB bonded magnet fabrication process. JOM 68:1978–1982. https://doi.org/10.1007/s11837-016-1883-4
11. Baldissera AB, Pavez P, Wendhausen PAP et al (2017) Additive manufacturing of bonded Nd–Fe–B—effect of process parameters on magnetic properties. IEEE Trans Magn 53:1–4. https://doi.org/10.1109/TMAG.2017.2715722
12. Li L, Tirado A, Nlebedim IC et al (2016) Big area additive manufacturing of high performance bonded NdFeB magnets. Sci Rep 6:36212. https://doi.org/10.1038/srep36212
13. Kolb T, Huber F, Akbulut B et al (2016) Laser beam melting of NdFeB for the production of reare-earth magnets. In: Proceedings of the EDCP conference 2016
14. Jaćimović J, Binda F, Herrmann LG et al (2017) Net shape 3D printed NdFeB permanent magnet. Adv Eng Mater 19:1700098. https://doi.org/10.1002/adem.201700098
15. Huber C, Sepehri-Amin H, Goertler M et al (2019) Coercivity enhancement of selective laser sintered NdFeB magnets by grain boundary infiltration. Acta Mater 172:66–71. https://doi.org/10.1016/j.actamat.2019.04.037
16. Goll D, Vogelgsang D, Pflanz U et al (2019) Refining the microstructure of Fe-Nd-B by selective laser melting. Phys Status Solidi RRL 13:1800536. https://doi.org/10.1002/pssr.201800536
17. Urban N, Meyer A, Kreitlein S et al (2017) Efficient near net-shape production of high energy rare earth magnets by laser beam melting. AMM 871:137–144. https://doi.org/10.4028/www.scientific.net/AMM.871.137
18. Magnetquech: "MQP-S-11-9-20001-070 isotropic powder" data sheet. https://mqitechnology.com/product/mqp-s-11-9-20001/
19. Rabinovich YM, Sergeev VV, Maystrenko AD et al (1996) Physical and mechnical properties of sintered Nd-Fe-B type permanent magnets. Intermetallics 4:641–645
20. Horton JA, Wright JL, Herchenroeder JW (1996) Fracture toughness of commercial magnets—magnetics. IEEE Trans Magn 32:4374–4376
21. Liu JF, Vora P, Walmer MH et al (2005) Microstructure and magnetic properties of sintered NdFeB magnets with improved impact toughness. J Appl Phys 97:10H101. https://doi.org/10.1063/1.1847215
22. Rösler J, Harders H, Bäker M (2006) Mechanisches Verhalten der Werkstoffe. Teubner, Wiesbaden
23. Macherauch E, Zoch H-W (2011) Praktikum in Werkstoffkunde. Vieweg+Taubner, Wiesbaden
24. Schrefl T, Fischer R, Fidler J et al (1994) Two- and three-dimensional calculation of remanence enhancement of rare-earth based composite magnets (invited). J Appl Phys 76:7053–7058. https://doi.org/10.1063/1.358026